ELSEVIER

International Journal of Thermal Sciences 41 (2002) 899–911

International Journal of Thermal Sciences

www.elsevier.com/locate/ijts

Solutal thermodiffusion in binary mixture in the presence of g-jitter

M. Chacha [a], D. Faruque [a], M.Z. Saghir [a,*], J.C. Legros [b]

[a] *Ryerson University, Department of Mechanical Engineering, 350 Victoria Street, Toronto, ON, L6H 5C2, Canada*
[b] *Université libre de Bruxelles, Brussels, Belgium*

Received 27 July 2001; accepted 27 November 2001

Abstract

The phenomenon of mass flux in a mixture due to a temperature gradient is known as the Soret effect or thermal diffusion. This effect is usually small but can be quite important in the analysis of compositional variation in hydrocarbon reservoirs. Diffusion-dominated experiments on-board the International Space Station will be greatly affected by convective flow due to the residual acceleration field and/or to oscillatory g-jitters caused by several sources. In this paper we are interested in investigating the flow due to thermal diffusion for different oscillatory g-jitters. The model considered is a rectangular rigid cavity filled with a binary mixture of methane and normal butane, subject to a temperature difference on its end walls and radiation heat transfer on the lateral ones. The non-linear differential equations for the mass-thermo-vibrational problem are derived in the case of a unique mode oscillatory acceleration. The full transient Navier–Stokes equations coupled with the mass and heat transfer formulations and the equation of state of the fluid are solved numerically using the finite element technique. Results revealed that the thermal diffusion is important and drives a strong convection. Convection is enhanced and therefore temperature and species profiles distortion from purely diffusive condition increases when a parallel g-jitter is added to the residual gravity, in a destabilizing configuration. The numerical study shows that both residual gravity and g-jitter may be detrimental but also beneficial to achieve purely diffusive conditions, according to the orientation of the vibration direction and the residual gravity vector, relative to the direction of the main density gradient. For the different configurations investigated, the g-jitter is found to reduce compositional variation. When the stable regime is attained, thermal and compositional quantities fluctuate following a mode whose frequency is equal to that of the initially imposed vibration. Even if the temperature fluctuation at a given point remains small, the compositional variation due to residual g-jitter convection is not negligible.

Keywords: Soret effect; Micro-gravity; g-jitter; Numerical simulation; Density calculation

1. Introduction

The phenomenon of mass flux in a mixture due to a temperature gradient is known as the Soret effect or thermal diffusion. This effect is usually small but can be quite important in the analysis of compositional variation in hydrocarbon reservoirs. In order to uncover the mechanism of compositional variation in a reservoir fluid, great efforts have been invested in the development of theoretical models as well as experimental set-ups. Because of buoyancy-induced convection in the gravitational field, accurate measurement of the Soret coefficient for multi-component mixtures is nearly impossible. Therefore an emergence of experimental set-up in micro-gravity environment becomes eminent. A joint micro-gravity experiment is planned by the authors to measure the Soret coefficient for a various multi-component oil system during a Space Shuttle mission. However, analysis of the effective acceleration environment on-board the Space Shuttle has shown that the residual acceleration field comprises a frequency spectrum. At frequencies of about 1 Hz, the amplitude is of the order of $10^{-4}g_0$ to $10^{-3}g_0$ where g_0 is the earth gravity magnitude, and increasing linearly with the frequency for higher frequencies [1]. The effect of such vibrations (called g-jitter), induced by on board machineries or excited by crew activities, on experiments conducted in space is largely unknown. Therefore, it is important to consider the effect of g-jitter in the analysis in order to better understand the micro-gravity experimental results.

Theoretical work concerning the instability in fluids under the influence of g-jitter in weightlessness conditions has been reported by several authors. Merkin [2], Davidson [3], Haddon and Riley [4] analyzed the instability in a liquid due to fluctuations of the acceleration field. They found

* Correspondence and reprints.
E-mail address: zsaghir@ryerson.ca (M.Z. Saghir).

1290-0729/02/$ – see front matter
PII: S1290-0729(02)01382-0

Nomenclature

a	interaction energy between molecules	$\mathrm{J\cdot m^3\cdot mol^{-2}}$
b	hard-core or co-volume parameter	$\mathrm{m^3\cdot mol^{-1}}$
c	transported component mass fraction (or concentration)	
c_0	initial butane concentration	
c_p	mixture specific heat	$\mathrm{J\cdot kg^{-1}\cdot K^{-1}}$
D^c	mass diffusivity	$\mathrm{m^2\cdot s^{-1}}$
D^M	molecular diffusivity	$\mathrm{m^2\cdot s^{-1}}$
D^p	pressure diffusion coefficient	$\mathrm{m^2\cdot s^{-1}\cdot Pa^{-1}}$
D^T	thermal diffusion coefficient	$\mathrm{m^2\cdot s^{-1}\cdot K^{-1}}$
f	frequency of the g-jitter	Hz
g_0	earth gravity acceleration magnitude	$\mathrm{m\cdot s^{-2}}$
g_1	magnitude of the static gravity (residual-g)	$\mathrm{m\cdot s^{-2}}$
g_2	amplitude of the g-jitter	$\mathrm{m\cdot s^{-2}}$
H_k	partial molar enthalpy of component k	$\mathrm{J\cdot mol^{-1}}$
$\vec{J}$	total mass flux	$\mathrm{kg\cdot m^{-2}\cdot s^{-1}}$
$\vec{J}_q$	heat flux	$\mathrm{W\cdot m^{-2}}$
k	mixture thermal conductivity	$\mathrm{W\cdot m^{-1}\cdot K^{-1}}$
k_{ij}	binary interaction parameter	
l_{ij}	binary interaction parameter	
L_{11}	phenomenological coefficient	$\mathrm{kg\cdot s\cdot K\cdot m^{-3}}$
L'_{1q}	phenomenological coefficient	$\mathrm{J\cdot s\cdot K\cdot m^{-3}}$
L	cavity length	mm
H	cavity height	mm
M	mixture molecular weight	$\mathrm{kg\cdot mol^{-1}}$
M_k	molecular weight of component k	$\mathrm{kg\cdot mol^{-1}}$
p	pressure	Pa
p_{T_m}	pressure at mean temperature	Pa
Q_k	heat of transport of the component k	$\mathrm{J\cdot mol^{-1}}$
R	universal gas constant 8.31441...	$\mathrm{J\cdot mol^{-1}\cdot K^{-1}}$
S^T	Soret coefficient	$\mathrm{1\cdot K^{-1}}$
t	time	s
T	temperature	K
T_0	room/initial temperature	K
T_c	cold wall temperature	K
T_h	hot wall temperature	K
T_m	mean temperature	K
T_r	reduced temperature	
u	velocity component in x-direction	$\mathrm{m\cdot s^{-1}}$
$\tilde{u}$	molar internal energy	$\mathrm{J\cdot mol^{-1}}$
$\bar{u}_k$	partial molar internal energy of component k	$\mathrm{J\cdot mol^{-1}}$
v	velocity component in y-direction	$\mathrm{m\cdot s^{-1}}$
$\tilde{v}$	molar volume	$\mathrm{m^3\cdot mol^{-1}}$
$\bar{v}_k$	partial molar volume of component k	$\mathrm{m^3\cdot mol^{-1}}$
x_1	mole fraction of the transported species	
x_i	mole fraction of component i	
x_k	mole fraction of component k	
Z	compressibility factor	

Greek symbols

ε	emissivity of the radiating walls	
μ	mixture dynamic viscosity	$\mathrm{kg\cdot m^{-1}\cdot s^{-1}}$
μ_k	chemical potential of component k	$\mathrm{J\cdot mol^{-1}}$
ω	acentric factor	
ρ	mixture mass density	$\mathrm{kg\cdot m^{-3}}$
σ	Stefan–Boltzmann constant	$5.67032\ \mathrm{W\cdot m^{-2}\cdot K^{-4}}$
τ_k	ratio of the energy of vaporization to the energy of viscosity of component k	
θ	angle between the vertical direction and the gravity field	rad

that convection induced by g-jitter resulted in a significant increase of the heat transport when compared with the purely diffusive distribution. In their studies the research was focused mainly on the onset of convection. Savino et al. [5] performed a three-dimensional numerical simulation on a fluid cell subject to periodic accelerations with a relatively high frequency. In their study, they focused only on the time averaged convective motion arising from thermovibrational effect.

Gershuni [6–8] and his co-workers reported a series of theoretical work in micro-gravity subject to the influence of vibrations, which was mainly focused on the flow instability. Later Gershuni et al. [9,10] investigated theoretically the vibrational convective instability for the case of an infinite 2D horizontal binary mixture layer, in the presence of the Soret effect. These attempts, based on linear analysis, resulted in the derivation of the convection stability limits and provided qualitative understandings of different instability mechanisms and forms. Efforts were made to extract precise qualitative as well as quantitative effect of thermal diffusion on convection in more realistic situations: low frequencies, arbitrary wave and multi-mode vibration. However, non-linearity—neglected in the preceding analysis—may become important to enhance the driving of the convection. Direct numerical simulations are essential tools for this purpose. Rees and Pop [11,12] studied the effect of g-jitter on free convection in porous media. Of particular importance, they quantified the influence of g-jitter's amplitude and frequency on the rate of heat transfer.

In this paper we study the Soret effect by performing a direct numerical analysis considering the effects of density variation (fluid compressibility) under the influence of vibrational instability in micro-gravity environment. We consider a finite two-dimensional binary mixture of methane

and n-butane (C_1/nC_4) subject to lateral temperature gradient including the Soret effect. In Section 2 we present the mathematical formulation of the problem in dimensional form. Section 3 presents the numerical procedure. In Section 4 we discuss the results obtained for different conditions. Section 5 concludes the results of this work. The appendix is devoted to the formulation and calculation of diffusion coefficients as well as the calculation of the density of the mixture using appropriate equation of state. To the best of our knowledge no work has been addressed to investigate the vibration effects on thermal diffusion.

2. Problem description and basic equations

In this section, we describe the basic equations and boundary conditions that govern the problem. The physical model of the cavity under study is sketched in Fig. 1(a). The system consists of a rectangular cavity containing a binary mixture. The cavity is subject to vibrations. These vibrations are due to the oscillatory component of the gravity called g-jitter. The cavity vibrations are thus modelled by a harmonic contribution to the body force. Two orientations of the gravity acceleration are considered: parallel and perpendicular to the thermal gradient. The cavity is allowed to exchange heat with its environment through radiation process at its top and bottom walls. The vertical walls are set to constant temperatures, T_h and T_c with T_h greater than T_c (horizontal thermal gradient). All walls are assumed to be rigid and impermeable to matter.

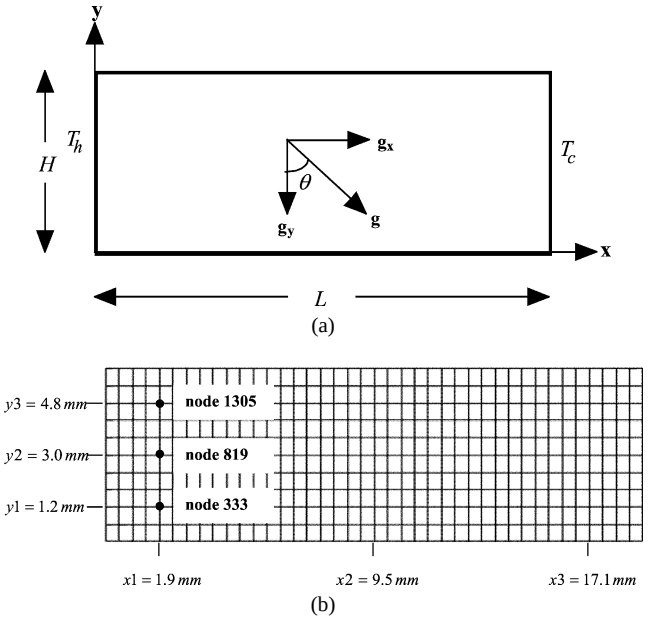

Fig. 1. Physical model and finite element mesh. (a) Physical model. (b) Finite element mesh and reported data analysis locations.

2.1. Mass conservation equation

The principle of mass conservation applied to a fluid, assuming a compressible flow in order to take into account the variation of the density, results in the following equation:

$$\frac{\partial \rho}{\partial t} + \frac{\partial \rho u}{\partial x} + \frac{\partial \rho v}{\partial y} = 0 \tag{1}$$

where ρ is the density, u and v are, respectively, the velocity component in the x and y directions, and t denotes the time.

Since the fluid is composed of two species, the principle of mass conservation applies to each individual component as well as to the mixture as a whole. For each component and in terms of the mass fraction c, the principle of mass conservation results in an equation of the form:

$$\rho\left(\frac{\partial c}{\partial t} + u\frac{\partial c}{\partial x} + v\frac{\partial c}{\partial y}\right) = -\vec{\nabla}\cdot\vec{j}$$
$$\vec{j} = -\rho\left[D^c\vec{\nabla}c - D^T\vec{\nabla}T\right] \tag{2}$$

where the total flux $\vec{j}$ comprises a Fickian diffusive flux (first term) and a thermal diffusive flux (second term). Eq. (2) is used for the solute conservation within the cavity, the second component (carrier-fluid) concentration being equal to $1 - c$. The terms D^c and D^T represent, respectively, the mass diffusivity and the thermal diffusion coefficient assumed to be constant in our analysis. The coefficients D^c and D^T deserve a particular attention since they are essential parameters for the process under investigation. The theoretical calculation of these coefficients is presented in the appendix, based on the thermodynamics of irreversible processes [13].

2.2. Momentum conservation equation

The principal of linear momentum is represented by the Navier–Stokes equations. In the x direction, this equation is written as:

$$\rho\left[\frac{\partial u}{\partial t} + u\frac{\partial u}{\partial x} + v\frac{\partial u}{\partial y}\right] = -\frac{\partial p}{\partial x} + \mu\left[\frac{\partial^2 u}{\partial x^2} + \frac{\partial^2 u}{\partial y^2}\right] + \rho g_x \tag{3}$$

Whereas in the y direction, the equation is written as:

$$\rho\left[\frac{\partial v}{\partial t} + u\frac{\partial v}{\partial x} + v\frac{\partial v}{\partial y}\right] = -\frac{\partial p}{\partial y} + \mu\left[\frac{\partial^2 v}{\partial x^2} + \frac{\partial^2 v}{\partial y^2}\right] + \rho g_y \tag{4}$$

where

$$g_x = \left[g_1 + g_2\sin(2\pi f t)\right]\sin\theta,$$
$$g_y = -\left[g_1 + g_2\sin(2\pi f t)\right]\cos\theta$$

We assume a periodical vibration, set only in one direction at a time: $\theta = 0$ or $\theta = -\pi/2$. θ is the angle between the negative y-axis and the gravity acceleration vector. The term g_1 is the magnitude of the residual gravity, while g_2 is

the amplitude of the gravity oscillating part (g-jitter) and f is the frequency of the oscillation. The pressure is denoted by p and μ is the dynamic viscosity of the mixture.

2.3. Energy conservation equation

Assuming no internal heat generation and constant thermal conductivity, the principle of conservation of thermal energy is expressed by the following equation:

$$\rho c_p \left[\frac{\partial T}{\partial t} + u\frac{\partial T}{\partial x} + v\frac{\partial T}{\partial y}\right] = k\left[\frac{\partial^2 T}{\partial x^2} + \frac{\partial^2 T}{\partial y^2}\right] \tag{5}$$

where c_p and k are, respectively, the specific heat and the thermal conductivity of the fluid and T is the temperature.

2.4. Equation of state

It is necessary to define the relationship of the density of the fluid to the flow parameters such as temperature, pressure, and species concentration in order to make use of the preceding conservation equations. This relationship is of the form:

$$f(\rho, p, T, c) = 0 \tag{6}$$

A specific paragraph is dedicated in the appendix to the calculation of the fluid density, which is performed using the Peng–Robinson equation of state [14].

2.5. Boundary conditions

The no-flow and no-slip boundary conditions are considered on the walls (Eq. (7)), which are not subject to surface reactions or mass flux (Eq. (8)). Constant yet different temperatures are imposed on the vertical walls and the horizontal walls are allowed to exchange heat through radiation with the surroundings (Eq. (9)). The boundary conditions are given below:

- Velocity boundary conditions

$$\begin{aligned} &u = v = 0 \qquad x = 0, \quad x = L \\ &u = v = 0 \qquad y = 0, \quad y = H \end{aligned} \tag{7}$$

- Species boundary conditions

$$\begin{aligned} &-D_c\frac{\partial c}{\partial x} + D_T\frac{\partial T}{\partial x} = 0 \qquad x = 0, \quad x = L \\ &-D_c\frac{\partial c}{\partial y} + D_T\frac{\partial T}{\partial y} = 0 \qquad y = 0, \quad y = H \end{aligned} \tag{8}$$

- Temperature boundary conditions

$$\begin{aligned} &T(x = 0, y) = T_h \qquad T(x = L, y) = T_c \\ &-k\frac{\partial T}{\partial y} = \varepsilon\sigma\left(T^4 - T_0^4\right) \qquad y = 0, \quad y = H \end{aligned} \tag{9}$$

where ε is the radiating surface emissivity, σ is the Stefan–Boltzmann constant, and T_0 is the temperature of the surroundings.

2.6. Initial conditions

The initial conditions are as follows (i.e., at time $t = 0$):

$$u(x, y) = v(x, y) = 0 \tag{10}$$

$$c = c_0 \tag{11}$$

$$T(x, y) = T_0 \tag{12}$$

3. Numerical procedure

We assume a single-phase fluid (liquid phase). All physical properties, except the fluid density, are constant with the assigned values obtained at mean temperature $T_m = (T_h + T_c)/2$. Table 1 lists the thermo-physical properties, the working conditions and the geometric data of the system used in the present numerical analysis. The working conditions are such that the pressure at mean temperature is $p_{T_m} = 350$ bar [15], where $T_m = 60\,^{\circ}\mathrm{C}$.

The numerical procedure consists of solving Eqs. (1)–(6) together with the appropriate boundary conditions (Eqs. (7)–(9)) by applying the Galerkin finite-element method for a variable density. The problem is strongly coupled since the density is related to the pressure, temperature and composition. The density is continually updated during the course of the solution procedure from the equation of state (Eq. (6)) at each mesh point. Following the initial flow field described by the initial conditions (Eqs. (10)–(12)), the time integration is performed using a first-order implicit scheme. The solution proceeds iteratively via a conjugate-gradient type iterative solver following the segregated approach (more cost-effective for considerable size or strongly coupled problems). The solution convergence is achieved at each time step and the iteration obtained once the relative error in the unknowns u, v, c and T for two successive iterations is less than 1×10^{-3}. Fig. 1(b) displays the mesh that was used to obtain all the results reported here: 40×10 second-order quadrilateral elements for a total of 1701 (81×21) nodes. The locations of interest in the results analysis are also shown in Fig. 1(b).

Table 1
Physical properties of the mixture and physical model data

T_h	338 K
T_m	333 K
T_c	328 K
μ	2×10^{-4} kg·m^{-1}·s^{-1}
k	0.095 W·m^{-1}·K^{-1}
p_{T_m}	35 MPa
c_p	2040 J·kg^{-1}·K^{-1}
D^c	5.88×10^{-9} m^2·s^{-1}
D^T	-5.0×10^{-12} m^2·s^{-1}·K^{-1}
$S^T = -D^T/D^c$	8.5×10^{-4} K^{-1}
L	19 mm
ε	0.1
T_0	303 K
H	6 mm

4. Results and discussion

Sources of the residual accelerations include the effects of the earth's gravity gradient and the g-jitter. The high-frequency accelerations may be unimportant in comparison with the residual motions caused by low frequencies. As a preliminary step towards complete investigation of the effects of vibrations on the mass-thermo-fluid dynamics of the binary mixture (C_1/nC_4), calculations have been performed for different cases. In the first case zero gravity condition is adopted, in the second case the g-jitter and/or residual gravity in x direction (i.e., $\theta = -\pi/2$) is applied and finally in the third case the g-jitter and/or residual gravity in y direction (i.e., $\theta = 0$) is studied. Three frequencies are investigated: $f = 0.1$, $f = 1$ and $f = 10$ Hz. When present, the steady residual acceleration (residual gravity) and the purely vibrational or oscillatory acceleration (g-jitter) are considered to be parallel. The initial mass fraction of n-butane is fixed to $c_0 = 0.8$. All the results are presented at time $t = 2025$ s after the thermal steady state condition is reached.

4.1. Influence of the residual gravity

In the present case, we are assuming that there is no g-jitter in the system. Fig. 2 shows the influence of the residual gravity on the thermo-diffusion in the absence of any oscillatory g-jitter at three horizontal lines situated at $y1$, $y2$ and $y3$ and passing, respectively, by nodes 333, 819 and 1305. The case denoted by $g0$ corresponds to the flow in the absence of any gravity (i.e., no residual gravity and no g-jitter, $g_1 = g_2 = 0$), while 0HzH, and 0HzV stand for the flow in the presence of a residual gravity (i.e., no g-jitter, $g_1 = 5 \times 10^{-5}$ m·s^{-2}, $g_2 = 0$) oriented towards negative x and negative y, respectively. The profiles are drawn for the lines passing by node 333 ($y1$), node 819 ($y2$) and node 1305 ($y3$).

In Fig. 2(a), non-linear temperature distributions are obtained due to the radiation heat losses along the horizontal walls. In fact, slight temperature differences do exist between the profile at the middle line ($y2$) and those off the middle line ($y1$ and $y3$). It is interesting to notice that the minimum temperature location is near the cold wall. It is evident that for this condition the line at $y = y2$ is a symmetry line for the temperature and species distribution. Therefore the results of the fluid temperature and the butane concentration at $y = y1$ and at $y = y3$ are identical.

Fig. 2(b) shows the butane concentration profiles at three horizontal planes $y1$, $y2$ and $y3$. For the sake of clarity some of those profiles are not represented. It was noted that the profiles at $y1$ and at $y3$ were identical, in the cases of zero-g and horizontal residual gravity. By comparing the butane distribution at $y1$ and $y2$, it is found that as we get closer to the cavity wall, more butane is located due to the loss of heat by radiation. In the presence of any residual gravity (cases 0HzH and 0HzV), it is found that low butane concentration

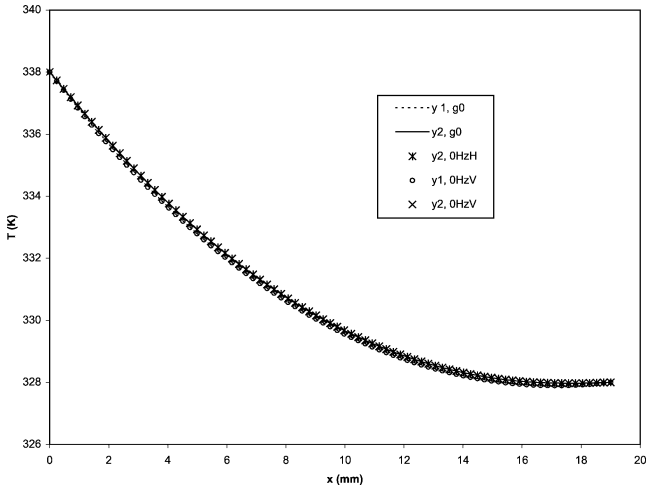

(a)

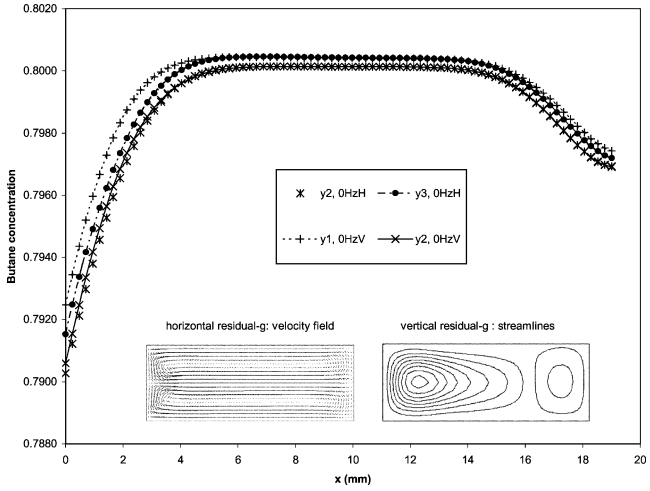

(b)

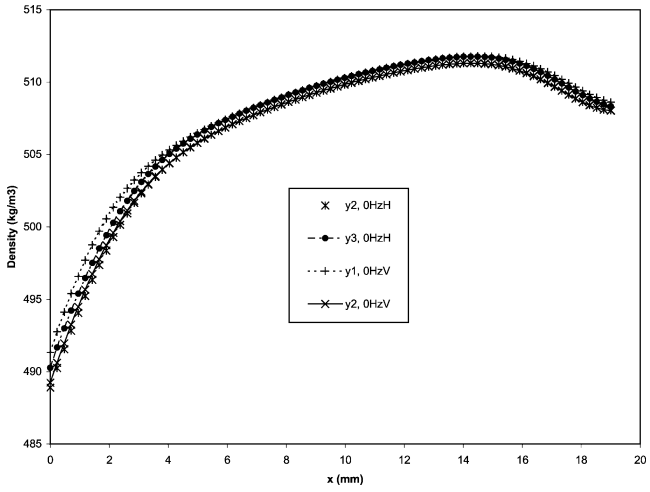

(c)

Fig. 2. Influence of residual-g on the diffusion processes. (a) Temperature profile. (b) Butane concentration. (c) Mixture density profile.

exists near the end walls compared to the central region of the cavity. The amount of butane on the cold end is however higher than that on the hot end. Two symmetric

rolls form apart from the line $y2$ in the presence of horizontal residual gravity. Fig. 2(b) (bottom) shows the corresponding flow structure illustrated by the velocity field. The maximum butane concentration is found to be near the radiating walls as in the previous case. However, the hot wall is now the location of minimum butane concentration as it is the case when any static gravity is accounted for. In the case of the downward residual gravity (i.e., 0HzV) the flow structure is asymmetrical. Two convection rolls are observed sustaining the presence of a minimal temperature cross-section. A large convective cell exists near the hot wall whereas a weak convective cell is near the cold end. A dissymmetry also appears in the butane distribution. The difference in the concentration distribution of the butane near the hot and cold end is due to the convective cell in the cavity. The strong convection near the hot wall developed a large concentration gradient of the butane. Whereas in the cold end of the cavity, where the convection is weaker, the concentration gradient is less pronounced. More butane is found to segregate into the lower part of the cavity (represented by the profile "$y1$, 0HzV"). The hot and the cold ends are concentration local minima.

Fig. 2(c) shows the influence of residual gravity on the mixture density. Profiles along x direction are drawn for the three planes which are $y1$, $y2$ and $y3$. In the case of zero gravity, the density variation is very smooth and is monotonically increasing from the hot end to the cold end (not shown). Variation of density at the two locations of $y2$ and $y1$ is minimal. When the residual gravity is present, the density increases to a maximum value situated at around $3/4$ of the cavity length and then decreases progressively to an intermediate value at the cold wall. The large density gradient near the hot wall is again due to the strong observed convection. While profiles $y1$ and $y3$ are symmetric in the case of horizontal residual gravity and represent higher density in comparison to the centre line $y2$, a dissymmetry is naturally found between $y1$ and $y3$ in the case of a downward residual gravity with denser fluid in the lower half of the cell.

The physics at zero gravity seem to differ from that at any residual gravity when heat losses are allowed on the lateral walls of the cell. In fact in the present case, the envelope of the butane concentration variation in the x direction is "concave" in zero gravity, while it is "convex" if any residual gravity is present. This is due to the convection in the cavity in the presence of residual gravity.

Cross-sectional temperature profiles are shown on Fig. 3(a) at $x1$, $x2$ and $x3$ (see Fig. 1(b)). The case with no-gravity condition is presented here. However, the trend was similar for those cases with a static gravity component ($g_1 = 5 \times 10^{-5}$ m·s^{-2}). Radiation losses on the lateral walls induce a lateral temperature gradient. Thus, as indicated in Fig. 3(a), non-linear temperature distributions were obtained. It is worth noticing that at the steady state the cold end temperature ($T_c = 328$ K) is still higher than the maximum temperature at $x3$; sustaining the influence of the heat losses.

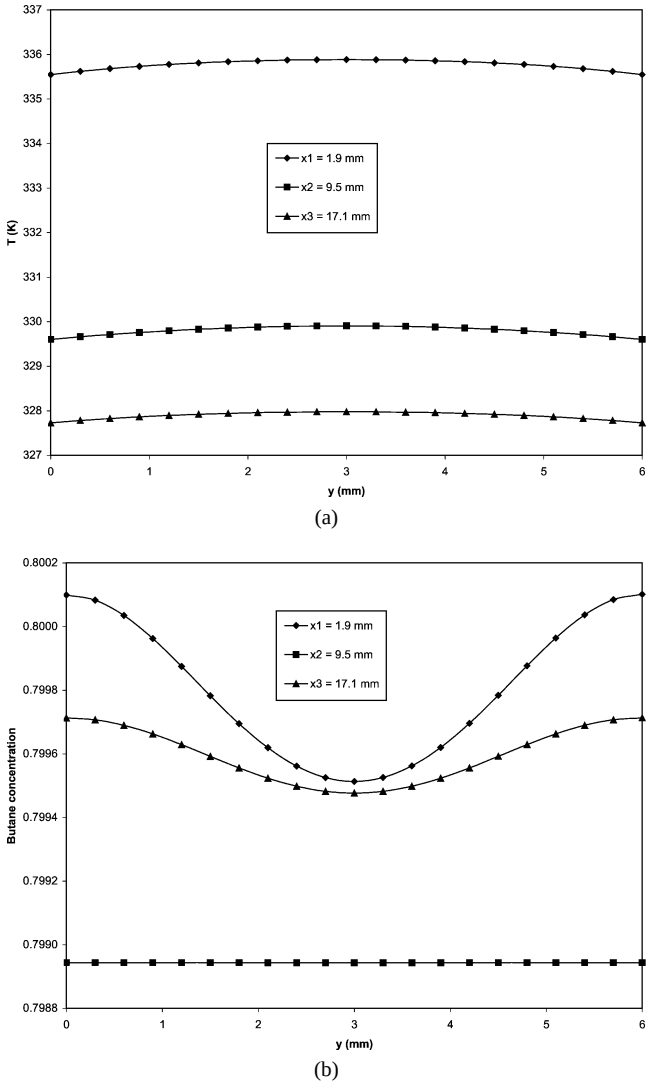

Fig. 3. Temperature and butane concentration profile under zero gravity condition. (a) Temperature profile. (b) Butane concentration profile.

Fig. 3(b) shows the butane concentration profile at different cross-sections ($x1$, $x2$ and $x3$) at zero gravity. The butane segregates towards the radiating walls while the methane migrates towards the central part of the cavity. This behaviour is expected from the fact that the Soret number is positive.

The previous case is repeated with a residual gravity applied in the horizontal and vertical direction, respectively. Under horizontal residual gravity, Fig. 4(a) shows the butane distribution at three different cross sections ($x1$, $x2$ and $x3$). High concentration of butane is found to be near the two horizontal walls and lower butane concentration is found at the centre of the cavity. The centre line at $y = y2$ is a symmetry line for the temperature and species distribution. Fig. 4(b) shows the same case but the residual gravity is oriented in the vertical direction. The convective flow is stronger and dominates over the thermodiffusion process, at

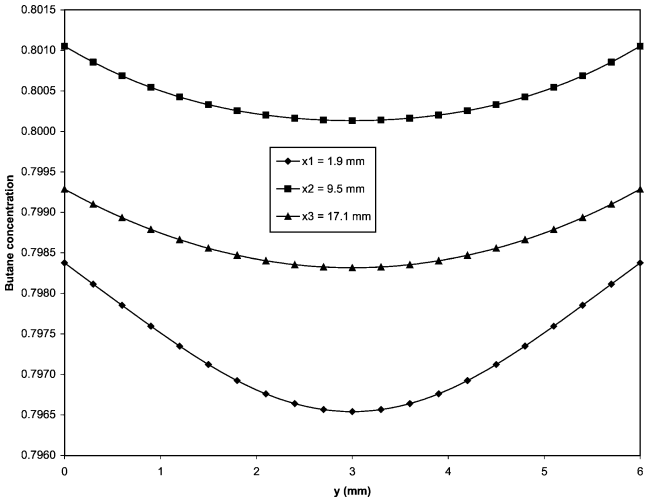

(a)

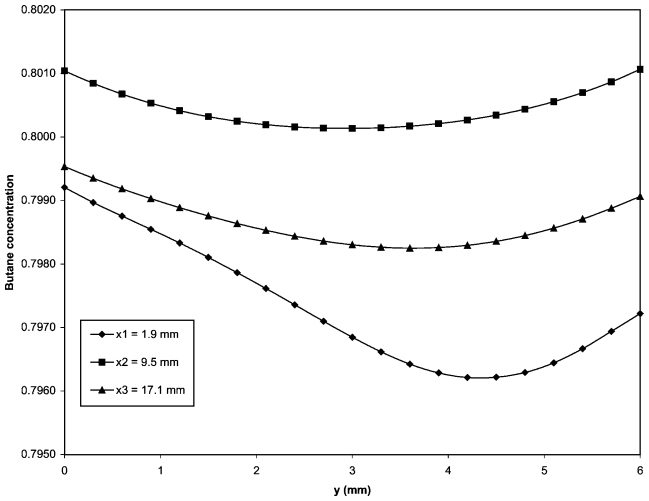

(b)

Fig. 4. Butane concentration under horizontal and vertical residual gravity. (a) Horizontal residual gravity. (b) Vertical residual gravity.

least on a considerable part of the cavity. The centre line is no more a line of symmetry for species distribution.

Whether the residual gravity is oriented horizontally or vertically, the mid-section corresponds to the highest butane concentration when compared to the other two sections at $x1$ and $x3$, respectively. On the contrary, under zero gravity condition (see Fig. 3(b)), the middle section (i.e., $x = x2$) corresponds to the lowest butane concentration level. We believe this is due to the fact that Soret effect is more pronounced in a zero gravity environment and is overcome by convection when the residual gravity is present. This in fact justifies the importance of measuring the Soret coefficient of a multi-component system in a zero gravity environment.

The centre line is found to be the loci for the minimal concentration in cross-sectional profiles for both zero gravity and horizontal residual gravity conditions. The minimum concentration location is not fixed in the case of a vertical residual gravity. Comparing longitudinal profiles to

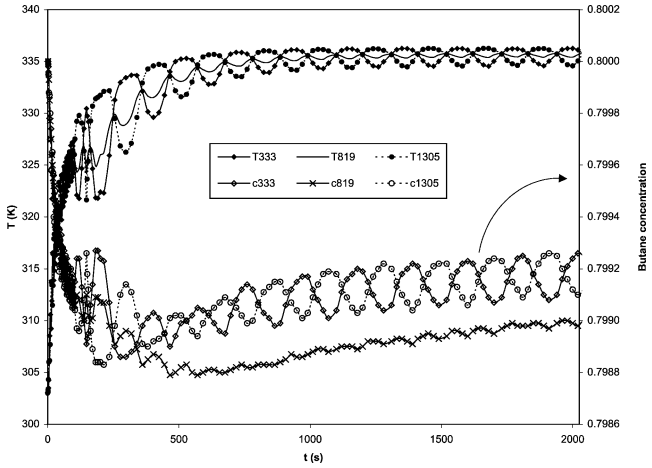

Fig. 5. Temperature and butane concentration time variation under a vertical vibration ($\theta = 0$, $f = 0.1$ Hz, time step is 21 seconds).

transversal ones, it is apparent that at zero gravity where no convection is observed, lateral segregation is very important and is even comparable to longitudinal segregation. It is obvious that when only residual gravity is present, the maximum deviation of the mass-thermo-fluid dynamic field from the purely diffusive situation (i.e., zero gravity) corresponds to a residual gravity vector orthogonal to the direction of the main temperature gradient. In this case convection develops for all values of the temperature difference between the hot and the cold ends and antagonises species separation by Soret diffusion.

4.2. *Influence of the frequency of the g-jitter*

In this case, the g-jitter implemented in Eqs. (3) and (4) will be adopted. The objective of this section is to examine the influence of frequency in the butane and temperature variation in the presence of the Soret effect. Three different frequencies will be used in our analysis. These are mainly 0.1, 1 and 10 Hz. The rational for using these frequencies is that we are interested in studying the effect of large frequency spectrum on the thermal diffusion. Fig. 5 shows the temperature and butane concentration variation in time at three specified nodes: 333, 819 and 1305. An oscillatory g-jitter having a frequency of $f = 0.1$ Hz is acting in the vertical direction in addition to the downward residual gravity. The temperature and concentration variation at the three nodes near the hot wall were investigated with time. While the temperature and the density (not shown) reach a periodical regime, the species concentration still undergoes an important activity. The average concentration continues to vary with time, tending asymptotically to a quasi-equilibrium value. In addition, a phase shift is noticeable for the temperature and the species concentration at off centre nodes (i.e., 333 and 1305). At the middle of the cavity (i.e., node 819), the temperature fluctuation in time can be considered negligible when a periodically stable regime is established in the flow. The density was found not

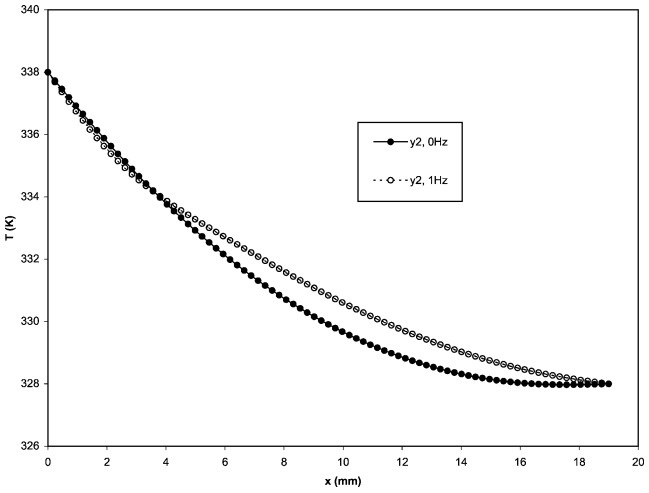

(a)

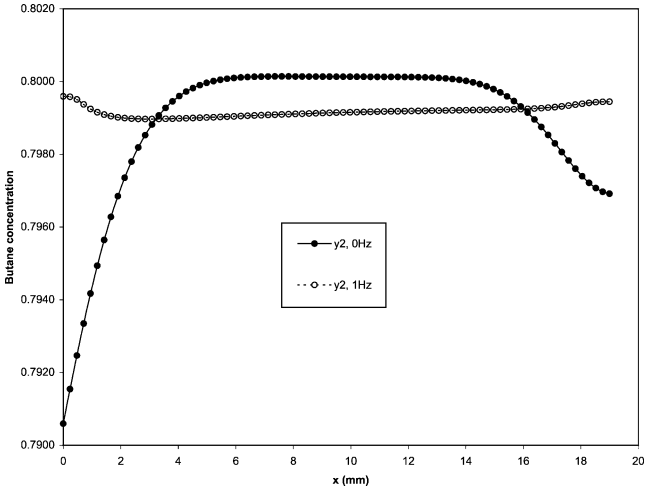

(b)

Fig. 6. Temperature and concentration profiles with g-jitter oriented vertically. (a) Temperature profile. (b) Concentration profile.

to be affected by the fluctuation of the composition and was found to depend on the temperature variation only.

Species diffusion (Soret and Fickian) is a slow process when compared to the heat diffusion process. By designating $\tau_{\text{th}} = \rho c_p L^2/k$ the heat transport characteristic time and $\tau_{\text{Fd}} = L^2/\pi^2 D^c$ the mass diffusion characteristic time [16], one may find that $\tau_{\text{th}} \leqslant \tau_{\text{Fd}}$. One could "speculate" that the average profile variation of the butane concentration with time is particularly attributable to thermo-diffusion process, while instantaneous fluctuations are due to the convection in the fluid.

Another way to examine the importance of the heat diffusion process versus the species diffusion is to present the temperature and the butane concentration at the middle of the cavity along its length. Fig. 6 represents the cases where an oscillatory g-jitter is added to the static gravity for a frequency $f = 1$ Hz. The gravity acceleration is directed along the y-axis with the static component downward ($\theta = 0$). Fig. 6(a) shows the influence of the g-jitter frequency on the

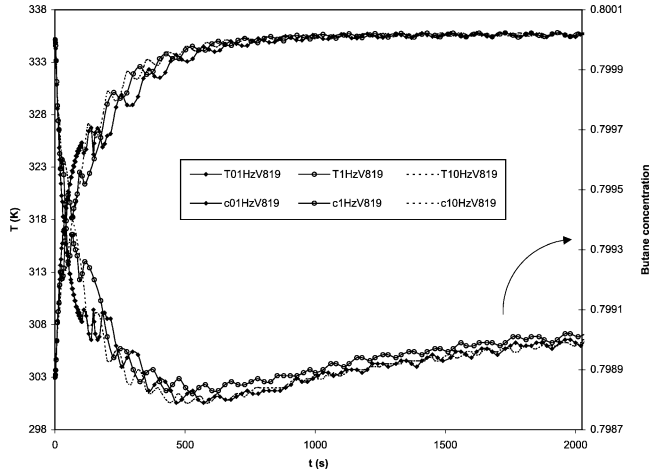

Fig. 7. Influence of the frequency of the g-jitter on the diffusion processes: temperature and butane variation at a mesh point.

temperature. A comparison between a residual gravity case and a g-jitter having a frequency of 1 Hz is presented. In the residual gravity case, a decrease in the temperature along the length of the cavity is noticeable. If we recall, our observation presented earlier showed that a lower temperature was found to be close to the cold end. This variation of temperature is mainly due to the radiation. In the presence of the g-jitter, disturbances create an additional mixing in the cavity and a quasi-linear temperature distribution in the cavity is noticeable. The minimum temperature is therefore displaced to the cold end. It was noticed that when a periodical regime is attained in the flow, the temperature at the mid-plane $y2$ is the same at every frequency; therefore only temperature profiles at 0 and 1 Hz are shown in Fig. 6(a).

Fig. 6(b) presents the butane concentration profile at two different cases at the mid-plane of the cavity. In the absence of g-jitter, the residual gravity directed downward shows a large butane concentration decrease near the hot wall due to the Soret effect. Let us recall that the g-jitter amplitude is 40 times greater than the residual gravity in the present study. In the presence of a g-jitter with a frequency of 1 Hz, mixing prevents Soret diffusion and lead to approximately constant butane concentration in the cavity. This finding shows again that g-jitter may create mixing and will overcome the Soret effect in a cavity. Therefore measuring the Soret coefficient in micro-gravity requires a zero gravity environment.

In order to examine the effect of the temperature and the butane variation with the g-jitter, Fig. 7 compares the results of these two variables at the mesh point (i.e., node 819) for the three different frequencies. For the temperature, it is important to notice that the frequency variation effect is negligible. However, for the butane concentration, one can definitely agree that low frequency g-jitter will have a tremendous effect on the butane distribution in the cavity. Therefore one may conclude that low and high frequency g-jitter will affect the Soret diffusion process in microgravity.

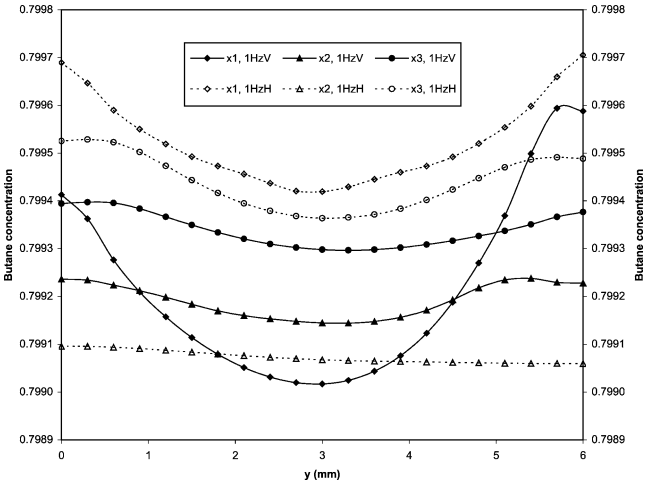

Fig. 8. Influence of the g-jitter direction on the diffusion processes at different cross-sections.

4.3. Influence of the direction

Up to now we have investigated the effect of temperature and butane concentration in the presence of g-jitter when the later is oriented in a vertical direction. In this section we intend to examine the previous case but where the orientation of both the g-jitter and the residual gravity is horizontal. Fig. 8 presents the variation of the butane at three different cross-sections of the cavity along the cavity height (i.e., $x1$, $x2$ and $x3$). In the presence of g-jitter having a frequency of 1 Hz and directed downward (i.e., HzV notation), a large variation of butane is observed. Mixing creates a non-uniform distribution of the butane. When horizontal g-jitter is applied at the same frequency (i.e., HzH notation), one may notice symmetry for the butane concentration between the upper and the lower part of the cavity. In addition, a high concentration of butane is found to be in the lower part of the cavity. Regardless whether the g-jitter is oriented vertically or horizontally, the Soret effect is eliminated due to this mixing which is coming from external disturbances.

Fig. 9 compares the time variation of the species concentration at three different mesh points: 333, 819 and 1305. The start-up is "chaotic" for both configurations. As we advance in time, differences appear progressively in the dynamics taking place in the two configurations. For the horizontally oriented gravity case, a multi-cellular convection is generated. A symmetrical convective cell with respect to the middle of the cavity is noticeable. By examining the concentration near the hot wall at three different nodes (i.e., 333, 819 and 1305) it is found that there is no phase shift by comparing the concentration between nodes 333 and 1305. The average concentration at node 819 is smaller than that of nodes 333 (or 1305), and the difference seems to remain constant in time. When the gravity is directed vertically, a single convective cell dominates the entire cavity. The concentration when examined at nodes 333 and 1305 has identical behaviours with a phase shift equal to π. The time variation of the average concentration in the vertical case is slower

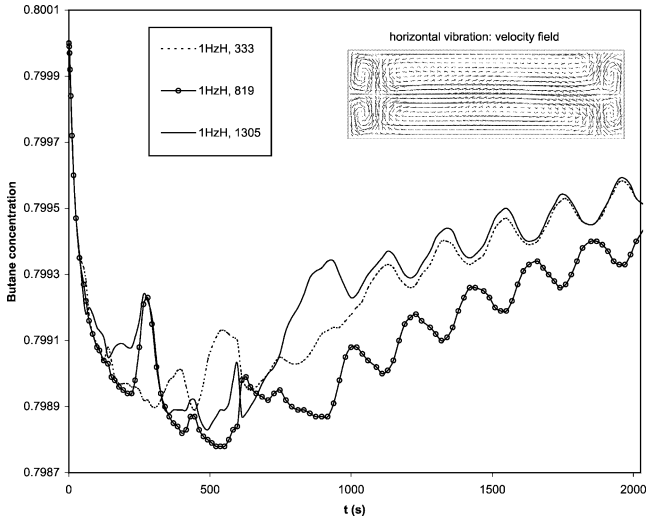

(a)

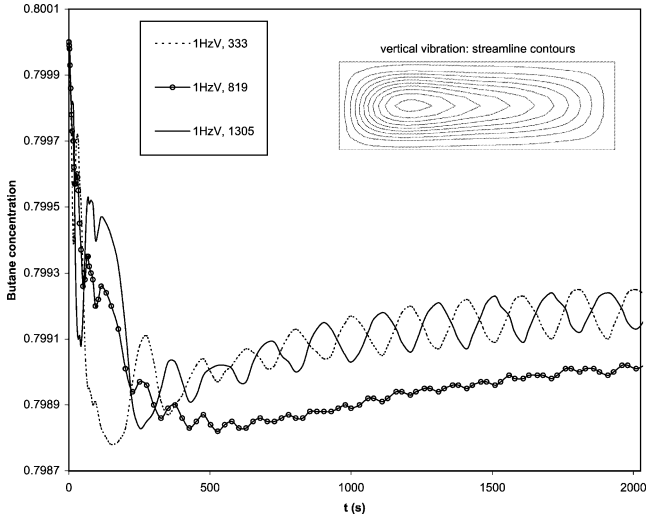

(b)

Fig. 9. Influence of the fluctuating gravity direction on the diffusion processes (time step is 15.1 seconds). (a) Gravity acceleration in the horizontal direction. (b) Gravity acceleration in the vertical direction.

than in the horizontal case. One may conclude that the orientation of the g-jitter is thus very critical to the mass transport process.

5. Conclusion

Static gravity (residual gravity) and oscillatory gravity (g-jitter) are unavoidable sources of convection during diffusion-dominated fluid science experiments on the International Space Station. We have investigated the role of thermal diffusion phenomena on compositional variation in a binary mixture of methane and normal butane in the presence of a fluctuating acceleration field. We considered a situation where the amplitude of the g-jitter is greater than the residual gravity. The mixture is contained in a rectangu-

lar cavity subject to heat losses on its horizontal walls and a temperature difference between its vertical walls.

In the absence of g-jitter, convection arises due to the presence of a residual gravity orthogonal to the main temperature gradient. The overall effect of the g-jitter is to reduce compositional variation. The presence of the g-jitter in the vertical or horizontal direction leads to the progressive remixing and therefore butane distribution tends to become uniform with increasing time. Remixing is stronger in the case of a fluctuating gravity field parallel to the main density gradient. Buoyancy and mass-thermo-vibrational effects can be completely eliminated, orienting the facility in such a way that the density gradient and the acceleration directions are aligned. When the g-jitter and the residual gravity act in the vertical direction (orthogonal to the main density gradient), the velocities are larger and the distortions of the isotherms from the purely diffusive situation reach the maximum.

Acknowledgement

We acknowledge the financial support of CRESTech, the Canadian Space Agency and the National Science and Engineering Research Council of Canada.

Appendix A

A.1. Density calculation

Optimal recovery of oil and natural gas relies to a considerable extent upon the knowledge of their thermodynamic properties. Cubic equations of state are widely used in reservoir simulation for this purpose, because of their computational simplicity. In our study, the (single-phase) fluid density is obtained at any point and time by solving the Peng–Robinson [12] cubic equation of state (PR CEOS).

A.1.1. The Peng–Robinson equation of state (PR EOS)

The Peng–Robinson [12] equation of state is:

$$p = \frac{RT}{\tilde{v} - b} - \frac{a}{\tilde{v}^2 + 2b\tilde{v} - b^2} \tag{A.1}$$

where R is the universal gas constant, $\tilde{v}$ is the molar volume, a is the interaction energy between molecules and, b is the hard-core or co-volume parameter and therefore, $\tilde{v}$ should be larger than b. The parameters a and b are obtained for a pure component from the critical temperature, critical pressure and the acentric factor as we will see later. For our mixture of 2 components, a and b are given by the following mixing rules:

$$a = \sum_{i=1}^{2}\sum_{j=1}^{2} x_i x_j a_{ij} \tag{A.2}$$

$$b = \sum_{i=1}^{2}\sum_{j=1}^{2} x_i x_j b_{ij} \tag{A.3}$$

where x_i is the mole fraction of component i.

The cross term parameters a_{ij} and b_{ij} are given by the following combining rules:

$$a_{ij} = (1 - k_{ij})\sqrt{a_{ii}a_{jj}} \tag{A.4}$$

$$b_{ij} = 0.5(b_{ii} + b_{jj})(1 - l_{ij}) \tag{A.5}$$

where a_{kk} and b_{kk} $(k = i, j)$ are, respectively, the interaction energy and co-volume of the pure component k. k_{ij} and l_{ij} are the binary interaction parameters. In our analysis, the parameter k_{ij} was made temperature dependant through the following relation:

$$k_{ij} = \gamma_{ij} + \frac{\chi_{ij}}{\sqrt{T}} \tag{A.6}$$

This functional form representing the temperature dependence of the binary interaction parameter k_{ij} was proposed by Fenghour et al. [17,18]. The optimal parameters of the PR EOS for a (methane + n-butane) system are: $\gamma_{12} = 0.0295$, $\chi_{12} = -8.817 \times 10^{-4}$ and $l_{12} = 0.0200$.

The volume correction or translation was introduced in our model. Previous works have shown that this last modification of the PR EOS can improve volumetric predictions for pure substances, except for supercritical compressed fluid (Peneloux et al. [18]; Jhaveri and Youngren [19]; Fenghour et al. [17]). For mixtures, a very satisfactory solution is not yet available (Firoozabadi [20]).

A.1.2. Parameters a and b in the PR EOS for pure components

To our knowledge, the latest improvement to the PR EOS parameters calculation is due to Twu et al. [21]. The ability of a CEOS to correlate the phase equilibrium of mixtures depends not only on the mixing rule, but also on the alpha function. These authors proposed a generalized temperature-acentric factor dependent function of the attractive term, called the alpha function. This generalized alpha function allows accurate reproduction of the vapour pressure data from the triple point to the critical point for hydrocarbons when used with the PR CEOS. The new PR EOS provides much more accurate and reliable vapour pressure predictions for light as well as heavy hydrocarbons than the original PR EOS.

For a pure component, the first and second derivatives of the pressure with respect to the volume are equal to zero at the critical point; that is:

$$\left.\frac{\partial p}{\partial \tilde{v}}\right|_{p=p_c,\,T=T_c} = 0, \qquad \left.\frac{\partial^2 p}{\partial \tilde{v}^2}\right|_{p=p_c,\,T=T_c} = 0 \tag{A.7}$$

These critical constraints give:

$$a(T_c) = 0.457235528921\frac{R^2T_c^2}{P_c} \tag{A.8}$$

$$b = 0.0777960739039\frac{RT_c}{P_c} \tag{A.9}$$

The subscript c denotes the critical condition, b is constant while a is a function of the temperature.

At temperatures other than critical temperature, the value of a (i.e., $a(T)$) is given by:

$$a(T) = a(T_c)\alpha(T_r, \omega) \tag{A.10}$$

The dimensionless parameter $\alpha(T_r, \omega)$ called the alpha function is the function that takes into account the attractive forces between the molecules. The reduced temperature is known to be $T_r = T/T_c$ and ω is the acentric factor. The first form of the alpha function was proposed by Soave [22]:

$$\alpha = \left[1 + m\left(1 - T_r^{0.5}\right)\right]^2 \tag{A.11}$$

where m is a 2nd (Peng and Robinson [12]) or a 3rd (Stryjek and Vera [23]) order polynomial in the acentric factor. This equation performs well for light hydrocarbons (acentric factors up to 0.5) at reduced temperatures between 0.7 and 1.0, but gives rise to significant errors at all temperatures for components with large acentric factors and the errors increase rapidly at low reduced temperatures for all components.

The development of the new generalized alpha function by Twu et al. [21] is based on the principle of corresponding states. The principle of corresponding states is a very useful tool for the prediction of the properties of a large class of substances from the knowledge of a few compounds. After selecting a group of compounds, which cover a wide range of acentric factors (mostly normal paraffin hydrocarbons), they first derived α as a function of temperature for each individual compound as:

$$\alpha = T_r^{N(M-1)}\, \mathrm{e}^{L(1-T_r^{NM})} \tag{A.12}$$

where L, M and N are unique to each component and have been determined from the regression of pure component vapour pressure. A plot of α vs. ω for a number of reduced isotherms showed a linear dependence of α on ω. A least-squares linear fit of α vs. ω finally yielded the generalized alpha function. α is finally expressed as a function of the reduced temperature and acentric factor ω as:

$$\alpha = \alpha^{(0)} + \omega\left(\alpha^{(1)} - \alpha^{(0)}\right) \tag{A.13}$$

where $\alpha^{(0)}$ and $\alpha^{(1)}$ correspond to $\omega = 0$ and $\omega = 1$, respectively.

For the sub-critical conditions ($T_r \leqslant 1$),

$$\alpha^{(0)} = T_r^{-0.171813}\, \mathrm{e}^{0.125283(1-T_r^{1.77634})} \tag{A.14}$$

$$\alpha^{(1)} = T_r^{-0.607352}\, \mathrm{e}^{0.511614(1-T_r^{2.20517})} \tag{A.15}$$

For the supercritical conditions ($T_r > 1$),

$$\alpha^{(0)} = T_r^{-0.792615}\, \mathrm{e}^{0.401219(1-T_r^{-0.992615})} \tag{A.16}$$

$$\alpha^{(1)} = T_r^{-1.98471}\, \mathrm{e}^{0.024955(1-T_r^{-9.98471})} \tag{A.17}$$

While the correlation was developed primarily using the data of n-paraffin hydrocarbons, it gives, relatively high accuracy for various other hydrocarbons as expected from the corresponding states principles.

A.1.3. Solving the PR CEOS

Close examination of the PR EOS exhibits three vertical asymptotes:

$$\tilde{v} = b \tag{A.18}$$

$$\tilde{v} = +\left(\sqrt{2} - 1\right)b \tag{A.19}$$

$$\tilde{v} = -\left(\sqrt{2} - 1\right)b \tag{A.20}$$

The only branch with physical meaning is that with $\tilde{v} > b$. The PR EOS can be rewritten:

$$Z^3 - (1 - B)Z^2 + \left(A - 3B^2 - 2B\right)Z - \left(AB - B^2 - B^3\right) = 0 \tag{A.21}$$

where

$$Z = \frac{p\tilde{v}}{RT} \tag{A.22}$$

$$A = \frac{ap}{R^2T^2} \tag{A.23}$$

$$B = \frac{bp}{RT} \tag{A.24}$$

This equation has only one root for $T_r > 1$ and three equal roots for $T_r = 1$. When $T_r \leqslant 1$, the cubic equation of state has three roots from which the complex roots are to be eliminated. If all the three roots are real roots, the smallest root corresponds to the liquid phase and the largest one to the vapour phase. The intermediate root has no physical meaning.

In our particular case, only one real root is obtained since our mixture is single-phase fluid. Thus, solving the cubic equation of state for Z, the compressibility factor, the mixture density is obtained from:

$$\rho = \frac{1}{\tilde{v}}M = \frac{p}{ZRT}M \tag{A.25}$$

where M is the mixture molar mass.

A.2. Diffusion coefficients calculation

Soret effect is important for the study of compositional variation in hydrocarbon reservoirs. Several theoretical models have been suggested to calculate thermal diffusion factors in binary mixtures with varying degrees of success. Among them, the model developed recently by Shukla and Firoozabadi [24] using irreversible thermodynamics got a remarkable attention. In the present work, we adopted Shukla–Firozabadi model in order to calculate thermal diffusion coefficient for the mixture under consideration.

In a fluid mixture consisting of two components at a given temperature T and pressure p, where the only external force is gravity, assuming that there is no heat generation, viscous dissipation or chemical reaction, de Groot and Mazur [13] proposed the entropy production to be written as:

$$\sigma = -\frac{1}{T^2}\left(\vec{J}_q - \sum_{k=1}^{2}\frac{\overline{H}_k}{M_k}\vec{J}_k\right)\cdot\vec{\nabla}T - \frac{1}{T}\sum_{k=1}^{2}\vec{J}_k\cdot\left(\vec{\nabla}_T\frac{\mu_k}{M_k} - \vec{F}\right) \tag{A.26}$$

where $\vec{J}_q$, M_k, $\overline{H}_k$, μ_k and $\vec{J}_k$ are heat flux, molecular weight, partial molar enthalpy, chemical potential and molar diffusion flux relative to molar average velocity of the component k, respectively. The term $\sum_{k=1}^{2}(\overline{H}_k/M_k)\cdot\vec{J}_k$ is the transfer of heat due to diffusion.

Defining

$$\vec{J}'_q = \vec{J}_q - \sum_{k=1}^{2}\frac{\overline{H}_k}{M_k}\vec{J}_k \tag{A.27}$$

and using $\vec{J}_1 + \vec{J}_2 = 0$, we can write

$$\sigma = -\frac{1}{T^2}\vec{J}'_q\cdot\vec{\nabla}T - \frac{1}{T}\vec{J}_1\cdot\vec{\nabla}_T\left(\frac{\mu_1}{M_1} - \frac{\mu_2}{M_2}\right) \tag{A.28}$$

From the concept of irreversible thermodynamics and molecular kinetic theory $\vec{J}_q$ can also be written as

$$\vec{J}_q = \frac{Q_1}{M_1}\vec{J}_1 + \frac{Q_2}{M_2}\vec{J}_2 \tag{A.29}$$

where Q_k is the heat of transport of the component k. $\vec{J}'_q$ then takes the form:

$$\vec{J}'_q = \frac{Q_1 - \overline{H}_1}{M_1}\vec{J}_1 + \frac{Q_2 - \overline{H}_2}{M_2}\vec{J}_2 = \frac{Q_1^*}{M_1}\vec{J}_1 + \frac{Q_2^*}{M_2}\vec{J}_2 \tag{A.30}$$

Substituting $\vec{J}'_q$ in the expression of entropy production strength and using $\vec{J}_1 + \vec{J}_2 = 0$ yields

$$\sigma = -\frac{1}{T}\left[\left(\frac{Q_1^*}{M_1} - \frac{Q_2^*}{M_2}\right)\frac{\vec{\nabla}T}{T} + \vec{\nabla}_T\left(\frac{\mu_1}{M_1} - \frac{\mu_2}{M_2}\right)\right]\cdot\vec{J}_1 \tag{A.31}$$

Since entropy production strength is a product of fluxes and driving forces and both of them are related to the same reference velocity, a linear relation exists between the forces and fluxes. Therefore we can write the phenomenological equations for the diffusion flux in the following two forms:

$$\vec{J}_1 = -L'_{1q}\frac{\vec{\nabla}T}{T^2} - \frac{1}{T}L_{11}\vec{\nabla}_T\left(\frac{\mu_1}{M_1} - \frac{\mu_2}{M_2}\right) \tag{A.32}$$

and

$$\vec{J}_1 = -\frac{1}{T}L_{11}\left[\left(\frac{Q_1^*}{M_1} - \frac{Q_2^*}{M_2}\right)\frac{\vec{\nabla}T}{T} - \vec{\nabla}_T\left(\frac{\mu_1}{M_1} - \frac{\mu_2}{M_2}\right)\right] \tag{A.33}$$

L'_{1q} and L_{11} are phenomenological coefficients called Onsager coefficients [25,26]. Comparing the fluxes we have

$$L'_{1q} = L_{11}\left(\frac{Q_1^*}{M_1} - \frac{Q_2^*}{M_2}\right) \tag{A.34}$$

The diffusive flux of component 1 (the transported component), $\vec{J}_1$, may be written in compact form as:

$$\vec{J}_1 = -\frac{\rho}{M}\left(D^M\vec{\nabla}x_1 + D^T\vec{\nabla}T + D^p\vec{\nabla}p\right) \tag{A.35}$$

where D^M is the molecular diffusivity, D^T is the thermal diffusivity, D^p is the pressure diffusivity. The molecular diffusivity is given by:

$$D^M = \frac{\tilde{v}RL_{11}}{M_2x_2}\left(\frac{M_1x_1 + M_2x_2}{M_1}\frac{\partial\ln f_1}{\partial x_1}\bigg|_{x_1,T,p}\right) \tag{A.36}$$

where

$$\ln f_1 = \int_{\infty}^{\tilde{v}}\left[\frac{1}{nRT}\left(\frac{\partial p}{\partial x_1}\right)_{T,\tilde{v},n_2} - \frac{1}{\tilde{v}}\right]\mathrm{d}\tilde{v} - \ln Z + \ln(x_1p) \tag{A.37}$$

f_1 is the fugacity of the transported component and is calculated directly from the equation of state, while n is the total number of moles of the mixture. Knowing the value of D^M one can evaluate the value of Onsager coefficient L_{11} from Eq. (A.36). The thermal diffusivity is then obtained as follows:

$$D^T = \frac{\tilde{v}MRL_{11}}{M_1x_1M_2x_2}\frac{k_{T_1}}{T} \tag{A.38}$$

$$k_{T_1} = \frac{M_1x_1M_2x_2}{MRTL_{11}}L'_{1q} = \frac{M_1x_1M_2x_2}{MRTL_{11}}\left(\frac{Q_1^*}{M_1} - \frac{Q_2^*}{M_2}\right) = \frac{x_1}{RT}Q_1^* \tag{A.39}$$

where we have used $\sum_{k=1}^{2}x_kQ_k^* = 0$. There is no need for D^p in the present analysis. We can calculate Q_k^* using the expression by Shukla and Firoozabadi [24] from the following expression

$$Q_1^* = -\frac{\bar{u}_1}{\tau_1} + \left[\frac{\bar{u}_1}{\tau_1} + \frac{\bar{u}_2}{\tau_2}\right]\frac{\bar{v}_1}{\tilde{v}} \tag{A.40}$$

$$Q_2^* = -\frac{\bar{u}_2}{\tau_2} + \left[\frac{\bar{u}_1}{\tau_1} + \frac{\bar{u}_2}{\tau_2}\right]\frac{\bar{v}_2}{\tilde{v}} \tag{A.41}$$

where $\bar{u}_k$, $\bar{v}_k$ and τ_k are the partial molar internal energy, partial molar volume and ratio of the energy of vaporization to the energy of viscosity of component k. $\bar{u}_k$ and $\bar{v}_k$ may be defined as:

$$\bar{u}_k = \left(\frac{\partial\tilde{u}}{\partial x_k}\right)_{T,p,x_{l,l\neq k}} \quad\text{and}\quad \bar{v}_k = \left(\frac{\partial\tilde{v}}{\partial x_k}\right)_{T,p,x_{l,l\neq k}} \tag{A.42}$$

The molar internal energy of the mixture, $\tilde{u}$, has the expression:

$$\tilde{u}(T,p) - \tilde{u}^*(T,0) = \int_{\infty}^{\tilde{v}}\left[T\left(\frac{\partial p}{\partial T}\right)_{\tilde{v}} - p\right]\mathrm{d}\tilde{v} \tag{A.43}$$

where $\tilde{u}^*(T,0)$ is the ideal gas molar internal energy at zero pressure and temperature T.

The molecular diffusion coefficient D^M may be calculated directly, following the method given by Kooijman et al. [27]. D^M is then converted into D^c using the following straightforward relationship involving the mixture molecular weight M, and the components molecular weights M_1 and M_2:

$$D^c = \frac{M^2}{M_1 M_2} D^M. \tag{A.44}$$

References

[1] W. Knable, D. Eilers, Low-gravity environment in spacelab, Acta Astronaut. 9 (1992) 187.
[2] J.H. Merkin, Oscillatory free convection from an infinite horizontal cylinder, J. Fluid Mech. 30 (1967) 561.
[3] B.J. Davidson, Heat transfer from a vibrating circular cylinder, Internat. J. Heat Mass Transfer 16 (1973) 1703.
[4] E.W. Haddon, N. Riley, The heat transfer between concentric vibrating circular cylinders, Quart. J. Mech. Appl. Math. 34 (1981) 345.
[5] R. Savino, R. Monti, M. Piccirillo, Thermovibrational convection in a fluid cell, Computers and Fluids 27 (1998) 923.
[6] G.Z. Gershuni, E.M. Zhukhovitsky, Free thermal convection in a vibrational field under conditions of weightlessness, Soviet Phys. Dokl. 24 (1979) 894.
[7] G.Z. Gershuni, E.M. Zhukhovitsky, Convective instability of a fluid in a vibrational field under conditions of weightlessness, Fluid Dynamics 16 (1981) 498.
[8] G.Z. Chernatinsky, G.Z. Gershuni, R. Monti, Transient regimes of thermovibrational convection in a closed cavity, Microgravity Quart. 3 (1993) 55.
[9] G.Z. Gershuni, A.K. Kolesnikov, J.C. Legros, B.L. Myznikova, On the vibrational convective instability of a horizontal binary-mixture layer with Soret effect, J. Fluid Mech. 330 (1997) 251.
[10] G.Z. Gershuni, A.K. Kolesnikov, J.C. Legros, B.L. Myznikova, On the convective instability of a horizontal binary-mixture layer with Soret effect under transversal high frequency vibration, Internat. J. Heat Mass Transfer 42 (1999) 547.
[11] D.A.S. Rees, I. Pop, The effect of g-jitter on vertical free convection boundary-layer flow in porous media, Internat. Commun. Heat Mass Transfer. 27 (2000) 415.
[12] D.A.S. Rees, I. Pop, The effect of g-jitter on free convection near a stagnation point in a porous medium, Internat. J. Heat Mass Transfer 44 (2001) 877.
[13] S.R. de Groot, Non-Equilibrium Thermodynamics, Dover, New York, 1984.
[14] D.Y. Peng, D.B. Robinson, A new two-constant equation of state, Ind. Eng. Chem. Fundam. 15 (1976) 58.
[15] Ph. Georis, F. Montel, S. Van Vaerenbergh, Y. Decroly, J.C. Legros, Measurement of the Soret coefficient in crude oil, SPE 50573 (1998) 57.
[16] G. Thomaes, L'Effet Soret Èlémentaire, Thèse de Doctorat, Université Libre de Bruxelles, Belgique, 1951.
[17] A. Fenghour, J.P.M. Trusler, W.A. Wakeham, Phase behaviour and density of (methane + n-butane), Fluid Phase Equilib. 139 (1999).
[18] A. Peneloux, E. Rauzy, R. Fréze, A consistent correction for Redlich–Kwong–Soave volumes, Fluid Phase Equilib. 8 (1982) 7.
[19] B.S. Jhaveri, G.K. Youngren, Three-parameter modification of the Peng–Robinson equation of state to improve volumetric predictions, SPE Res. Engrg. 1033 (1988).
[20] A. Firoozabadi, Thermodynamics of Hydrocarbon Reservoirs, McGraw-Hill, New York, 1999.
[21] C.H. Twu, J.E. Coon, J.R. Cunningham, A new generalized alpha function for a cubic equation of state part 1. Peng–Robinson equation, Fluid Phase Equilib. 105 (1995) 49.
[22] G. Soave, Equilibrium constants from a modified Redlich–Kwong equation of state, Chem. Engrg. Sci. 27 (1972) 1197.
[23] R. Stryjek, J.H. Vera, An improved equation of state, in: K.C. Chao, R.L. Robinson (Eds.), Equations of State: Theories and Applications, ACS Symposium Ser. 300, American Chemical Society, Washington.
[24] K. Shukla, A. Firoozabadi, A new model of thermal coefficients in binary hydrocarbon mixtures, Ind. Engrg. Chem. Res. 37 (1998) 3331.
[25] L. Onsager, Reciprocal relations in irreversible processes: I, Phys. Rev. 37 (1931) 405.
[26] L. Onsager, Reciprocal relations in irreversible processes: II, Phys. Rev. 38 (1931) 2265.
[27] H.A. Kooijman, R. Taylor, Estimation of diffusion coefficients in multicomponent liquid systems, Ind. Engrg. Chem. Res. 30 (1991) 1217.